



**HAL**  
open science

# Direct-impact Hopkinson tests on the Ti-6Al-4V alloy at very high strain rate and inverse identification of elastic-viscoplastic constitutive models

Xiaoli Guo, Thomas Heuzé, Guillaume Racineux, Ramzi Othman

## ► To cite this version:

Xiaoli Guo, Thomas Heuzé, Guillaume Racineux, Ramzi Othman. Direct-impact Hopkinson tests on the Ti-6Al-4V alloy at very high strain rate and inverse identification of elastic-viscoplastic constitutive models. 22e Congrès Français de Mécanique, Aug 2015, Lyon, France. hal-02279962

**HAL Id: hal-02279962**

**<https://hal.science/hal-02279962>**

Submitted on 5 Sep 2019

**HAL** is a multi-disciplinary open access archive for the deposit and dissemination of scientific research documents, whether they are published or not. The documents may come from teaching and research institutions in France or abroad, or from public or private research centers.

L'archive ouverte pluridisciplinaire **HAL**, est destinée au dépôt et à la diffusion de documents scientifiques de niveau recherche, publiés ou non, émanant des établissements d'enseignement et de recherche français ou étrangers, des laboratoires publics ou privés.



Distributed under a Creative Commons Attribution 4.0 International License

# Direct-impact Hopkinson tests on the Ti-6Al-4V alloy at very high strain rate and inverse identification of elastic-viscoplastic constitutive models

X. Guo<sup>a</sup>, T. Heuzé<sup>a</sup>, G. Racineux<sup>a</sup>, R. Othman<sup>b</sup>

a. Research Institute in Civil and Mechanical Engineering (GeM, UMR 6183 CNRS), École Centrale de Nantes, 1 rue de la Noë, 44321 Nantes cedex 3, France. {Xiaoli.Guo, Thomas.Heuze, Guillaume.Racineux}@ec-nantes.fr

b. Mechanical engineering department, Faculty Engineering, King Abdulaziz University, P.O.BOX, 80248, Jeddah, 21589, Saudi Arabia. Ramzi.Othman@ec-nantes.fr

## Résumé :

*Ce travail a pour but de caractériser le comportement de l'alliage Ti-6Al-4V à très haute vitesse déformation. Pour cela, nous avons conçu et dimensionné un système de Hopkinson à impact direct et pu balayer des vitesses de déformation comprises entre  $3000s^{-1}$  et  $25000s^{-1}$ . Les lois élastique-viscoplastiques de Johnson-Cook, Zerilli-Armstrong et Nouaillhas ont été identifiées sur la base des données expérimentales par analyse inverse. Ces trois lois permettent de bien décrire les données expérimentales dans une gamme allant de  $3000s^{-1}$  à  $18000s^{-1}$ .*

## Abstract :

*The dynamic behaviour of the Ti-6Al-4V alloy is studied experimentally and numerically in this work. Using a direct-impact device, dynamic tests done on a wide range of strain rate of  $3000$  to  $25000s^{-1}$  are succeeded on this alloy. An inverse analysis involving a numerically dynamic analysis is then adopted for identifying three elastic-viscoplastic constitutive models on the dynamic tests : the Johnson-Cook, Zerilli-Armstrong and Nouaillhas models. The results show that all these models fit well the experimental data at a strain rate up to  $18000s^{-1}$ .*

**Mots clefs : Direct impact Kolsky bar ; Inverse analysis ; High strain rate ; elastic-viscoplastic constitutive models**

## 1 Introduction

The study of the material performance at high strain rate is an important topic in material sciences, since the materials usually exhibit strong viscous effects as the rate rises. In some material processes, the metallic materials may experience very high strain rates up to  $10^6s^{-1}$ , such as the laser shock peening [1]. Studying the dynamic behaviour of the materials requires to perform dynamic tests on a wide range of strain rate. The classical Split Hopkinson Pressure Bar (SHPB), also referred to as the Kolsky bar [2, 3], is the most widely used apparatus to perform such dynamic tests. The classical SHPB device is capable to attain strain rates ranging from  $10^2$  to  $10^4s^{-1}$  [4, 5]. Attempting to reach higher strain rate may yield the incident bar. Thus a direct-impact Hopkinson device has been developed [6] by removing the incident bar. On this direct-impact device, a very high strain rate of the order of  $10^5s^{-1}$  is achieved by [6] and [7]. In this work, the Ti-6Al-4V alloy is tested on a direct-impact Hopkinson device at strain rates ranging from  $3000$  to  $25000s^{-1}$ . Then an inverse identification is carried out to identify three elastic-viscoplastic constitutive models for the Ti-6Al-4V on this wide range of strain rates.

## 2 Direct-impact tests on the Ti-6Al-4V at very high strain rate

The dynamic tests are performed on a dedicated direct-impact device which design is solution of an optimization problem as detailed in [8]. This device consists mainly of a transmitted bar, the projectile and the compulsory systems

for the measurement. The transmitted bar is 1.2m length and 10mm diameter. To compress the specimen on a wide range of strain rate, four projectiles are manufactured, of diameter 15.8mm and lengths of 500mm, 125mm, 60mm and 30mm respectively. The bar and the projectiles are all made of a high strength steel, MARVAL X2NiCoMo18-8-5, with a yield stress of 1800MPa. Three Wheastone bridges of double gauges are mounted along the bar length to measure the elastic strain and monitor the dispersion. Two laser diodes are equipped to measure the impact velocity of the projectile. A high speed camera is also equipped to observe the compression of the specimen and the movement of the projectile during the impact.

The experimental plan comes down to determine the value of the specimen length  $l_s$ , the projectile length  $l_p$  and its impact velocity  $v_p$ . However, the combination of these three parameters is not unique to attain the expected strain rate. Provided the expected strain rate  $\dot{\epsilon}_s$  and the allowable strain  $\epsilon_s$  in the specimen, their maximum values can be approximated through the following equations,  $c_p$  being the sound speed in the projectile :

$$\dot{\epsilon}_{s_{\max}} \approx \frac{v_p}{l_s} \quad , \quad \epsilon_{s_{\max}} \approx \dot{\epsilon}_s \frac{2l_p}{c_p} \quad (1)$$

The combination of the parameters for each objective strain rate is presented in table 1.

TABLE 1: Experimental plan and results

| Test n° | Obj. $\dot{\epsilon}$ ( $s^{-1}$ ) | $v_p$ (m/s) | $l_p$ (mm) | $l_s$ (mm) | $\dot{\epsilon}_{\max}$ ( $s^{-1}$ ) | $\epsilon_{\max}$ | Test n° | Obj. $\dot{\epsilon}$ ( $s^{-1}$ ) | $v_p$ (m/s) | $l_p$ (mm) | $l_s$ (mm) | $\dot{\epsilon}_{\max}$ ( $s^{-1}$ ) | $\epsilon_{\max}$ |
|---------|------------------------------------|-------------|------------|------------|--------------------------------------|-------------------|---------|------------------------------------|-------------|------------|------------|--------------------------------------|-------------------|
| T1      | 3000                               | 15          | 500        | 5          | 3064                                 | 11%               | T7      | 18000                              | 36          | 60         | 2          | 17970                                | 33%               |
| T2      | 5000                               | 25          | 125        | 5          | 4642                                 | 16%               | T8      | 18000                              | 30          | 60         | 1.5        | 18350                                | 16%               |
| T3      | 7000                               | 28          | 125        | 4          | 6925                                 | 17%               | T9      | 20000                              | 30          | 60         | 1.5        | 21222                                | 23%               |
| T4      | 10000                              | 30          | 60         | 3          | 10740                                | 17%               | T10     | 20000                              | 40          | 30         | 2          | 19659                                | 24%               |
| T5      | 12000                              | 36          | 60         | 3          | 12040                                | 25%               | T11     | 25000                              | 37.5        | 30         | 1.5        | 25050                                | 25%               |
| T6      | 15000                              | 30          | 60         | 2          | 15010                                | 11%               |         |                                    |             |            |            |                                      |                   |

The measured data consist of the elastic strain  $\epsilon_b(t)$  in the transmitted bar and the impact velocity  $v_p$  of the projectile. The force  $F_s(t)$  applied by the bar on the specimen is computed from the recorded strain  $\epsilon_b(t)$  by  $F_s(t) = E_b S_b \epsilon_b(t)$ , where  $E_b$  and  $S_b$  are the Young's modulus and the cross-section of the bar. The force  $F_s(t)$  computed for the tests listed in table 1 is plotted in the figure 1 for each projectile length. In these curves, some trays are observed during the unloading part. These arise from (i) the shorter length of the projectile than that of the bar and (ii) the mismatch of the *generalized wave impedances* [9] of the projectile  $(\rho c S)_p$ , the specimen  $(\rho c S)_s$  and the transmitted bar  $(\rho c S)_b$ . Moreover, when the projectile is long enough, the loading time is equivalent to the characteristic time, as shown in the figure 1(a) where the projectile is 500mm length. As the projectile length shortens, the actual period of the compression of the specimen lasts approximately twice the characteristic time or even longer as observed in the figures 1(b)-1(d), resulting from the different cross-sections of the projectile and the bar in these experiments. As a consequence, the specimen in these tests experiences a second-time compression before the unloading wave arrives, and thus obtained a greater residual strain than that of the test T1 as shown in the table 1, even though the greatest kinematic energy is achieved in this test.

Without any input bar to measure the input force, the strain rate in the specimen is assessed by the following equation [4, 8] :

$$\dot{\epsilon}_s(t) = - \frac{v_p + \frac{S_p + S_b}{S_p} c_b \epsilon_b(t)}{l_s} \quad (2)$$

where  $S_p$  and  $c_b$  are the cross-section of the projectile and the sound speed of the bar. The maximum compressive strain rate  $\dot{\epsilon}_{\max}$  assessed by this equation and the measured compressive strain  $\epsilon_{\max}$  are presented in table 1 for each test. According to this formula, the compressive strain rate gets its extremum equal to  $v_p/l_s$  at the beginning of the impact. However, this equation is only valid within the characteristic time [4].

The stress-strain curves are thus assessed using the classical analysis of the Hopkinson tests [10] as shown in the figure 2. The curves exhibit a rising strain hardening as the strain rate increases. They are subject to scattering, as we

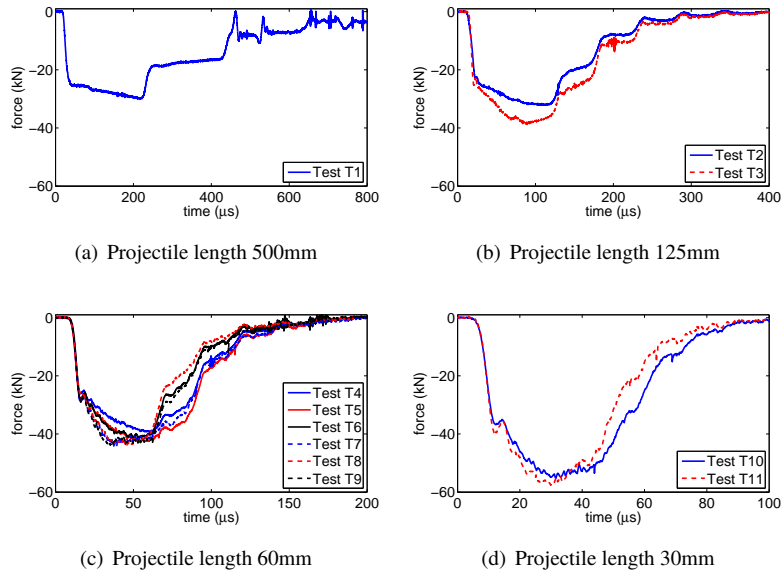


FIGURE 1: Force on the specimen in the direct-impact tests

can observe through small oscillations and a smaller flow stress appear in the curves of the tests T8 and T9. Oscillations are also observed at higher strain rate in the figure 2(d). Consequently, the rate dependency is difficult to be assessed on these curves directly. An inverse analysis is carried out for the identification of the constitutive models.

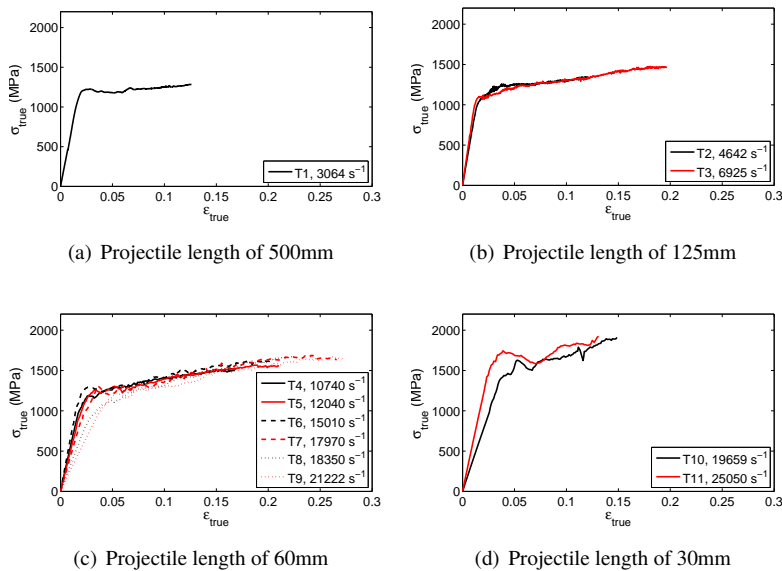


FIGURE 2: Stress-strain curves of the Ti-6Al-4V

### 3 Inverse identification of elastic-viscoplastic constitutive models

Three elastic-viscoplastic constitutive models have been chosen for their potential abilities to fit correctly the experimental measurements and are identified by means of an inverse procedure involving a dynamic numerical analysis.

No thermal effect is addressed in these identifications. The Johnson-Cook model [11] in isothermal conditions reads :

$$\sigma(p, \dot{p}) = (A + Bp^n) \left( 1 + C \ln \frac{\dot{p}}{\dot{p}_0} \right) \quad (3)$$

where  $p$  and  $\dot{p}$  are the cumulated plastic strain and strain rate respectively. The parameters  $A$ ,  $B$  and  $n$  are identified on quasi-static stress-strain curves obtained at the strain rate of  $10^{-4} s^{-1}$  [10] :  $A=955\text{MPa}$ ,  $B=770\text{MPa}$  and  $n=0.557$ . Thus only the parameter  $C$  is to be identified in the inverse process. An axisymmetric 2D Finite Element model in ABAQUS is created to proceed the dynamic simulation, consisting of the projectile, the specimen and the bar all meshed. The Zerilli-Armstrong model [12] is calibrated on the same experimental database, using a unidimensional FE model in MATLAB developed by [13]. Two variants for bcc and hcp materials are considered, that read :

$$\sigma_y = C_0 + C_1 \exp(-C_3 T + C_4 T \ln \dot{p}) + C_5 p^n \quad (\text{bcc}) \quad (4)$$

$$\sigma_y = C_0 + C_1 \exp(-C_3 T + C_4 T \ln \dot{p}) + C_2 \sqrt{\dot{p}} \exp(-C'_3 T + C'_4 T \ln \dot{p}) \quad (\text{hcp}) \quad (5)$$

Assuming a constant  $T$ , the first formula (4) reduces to :

$$\sigma_y = K_0 + K_1 p^n + K_2 \dot{p}^{K_3} \quad (\text{bcc}) \quad (6)$$

where  $K_0 = C_0$ ,  $K_1 = C_5$ ,  $K_2 = C_1 \exp(-C_3 T)$  and  $K_3 = C_4 T$ . The parameters  $K_0$ ,  $K_1$ ,  $n$  have the same value as the parameters  $A$ ,  $B$ ,  $n$  of the Johnson-Cook relation because of the equivalent form of strain hardening. Only two parameters  $K_2$  and  $K_3$  have been calibrated inversely. The second formula (5) reduces to :

$$\sigma_y = K_0 + K_1 \dot{p}^{K_2} + K_3 \sqrt{\dot{p}} \dot{p}^{K_4} \quad (\text{hcp}) \quad (7)$$

where  $K_0 = C_0$ ,  $K_1 = C_1 \exp(-C_3 T)$ ,  $K_2 = C_4 T$ ,  $K_3 = C_2 \exp(-C'_3 T)$  and  $K_4 = C'_4 T$ .  $K_0$  is equivalent to the yield stress, hence the unknown vector consists of four parameters  $K_1$ ,  $K_2$ ,  $K_3$  and  $K_4$  during the inverse identification. The Nouailhas model [14] has been used with success for adhesively bonded assemblies to account for viscous effects [15]. The creep law of this model is expressed as :

$$\dot{p} = \left\langle \frac{|\sigma| - R - \sigma_y}{K} \right\rangle^n \exp \left( \alpha \left\langle \frac{|\sigma| - R - \sigma_y}{K} \right\rangle^{n+1} \right) \quad (8)$$

where  $\langle x \rangle$  denotes the positive part of  $x$ , that is  $\langle x \rangle = \frac{x+|x|}{2}$ . The parameter  $\alpha$  enables to saturate the viscous effects. An isotropic hardening power law [16]  $\dot{R} = Q \dot{p}^m$  is adopted. The first three parameters  $\sigma_y$ ,  $Q$ ,  $m$  are also calibrated on the quasi-static tests from [10] :  $\sigma_y = 955\text{MPa}$ ,  $Q = 770\text{MPa}$ ,  $m = 0.557$ . The material parameters associated to the rate dependency are thus  $K$ ,  $n$  and  $\alpha$ .

The cost function  $f(\mathbf{x})$  is defined as the euclidean norm of the difference between the simulated strain  $\varepsilon_{\text{sim}}(\mathbf{x}, t)$  extracted at the location of the gauge and the recorded one  $\varepsilon_{\text{exp}}(t)$ . The identification is proceeded on each tests of the table 1 ; the calibrated strain  $\varepsilon_{\text{sim}}$  of the tests T1, T4, T6, T8 and T11 are plotted and superposed on the experimental one  $\varepsilon_{\text{exp}}$  in the figures 3(a)-3(e). An error bar is drawn associated to each mean value of the parameter  $C$  for the 2D identification, as shown in the figure 3(f), since at least two repetitions are carried out for each test. The simulated strains of different constitutive models are quite well superposed with the experimental one at strain rate up to  $15000 s^{-1}$ . A good concordance is observed at the second raising stage when the specimen is plastically deformed as shown in the figures 3(a)-3(c). Small discrepancy appears at this stage between the calibrated strain of the Johnson-Cook model and the measured one in the figure 3(d), whereas the Zerilli-Armstrong fits well the experimental data. As the strain rate goes higher, a greater strain is obtained from the test, while an equivalent amplitude of strain is simulated by the two constitutive models as presented in the figure 3(e). The figure 3(f) indicates that an approximately constant value of the parameter  $C$  of the Johnson-Cook model is identified at the strain rate ranging from  $3000$  to  $18000 s^{-1}$ . However a much greater value is obtained at very high strain rate in the tests T10 and T11. The discrepancies in these two tests may be due to (i) the very short projectile used in the test and/or (ii) the thermal effects not addressed in the identification. More repetitions of these two tests are to be carried out to enforce or not the results.

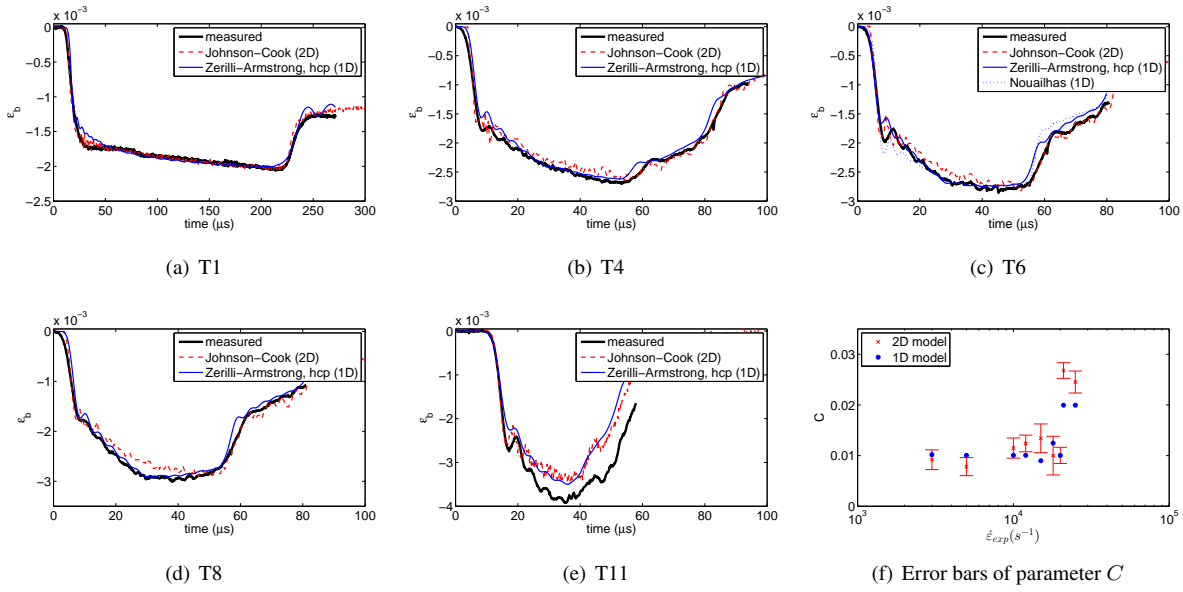


FIGURE 3: Results of the identifications

The stress-strain curves of the identified constitutive models are plotted at the strain rate of  $3000s^{-1}$  and  $18000s^{-1}$  and superposed to those obtained from the quasi-static tests in the figure 4. The figures 4(a)-4(c) show a great raise of the flow stress from the quasi-static to the dynamic conditions. But a much slighter increase is observed when the strain rate goes from 3000 to  $18000s^{-1}$ , especially for the Johnson-Cook model, where the two curves at these two strain rates are almost superposed in the figure 4(a). Indeed the rate dependency of this alloy has not been found greater than that predicted by the Johnson-Cook model at least in the studied range of strain rate, and so does for the other models.

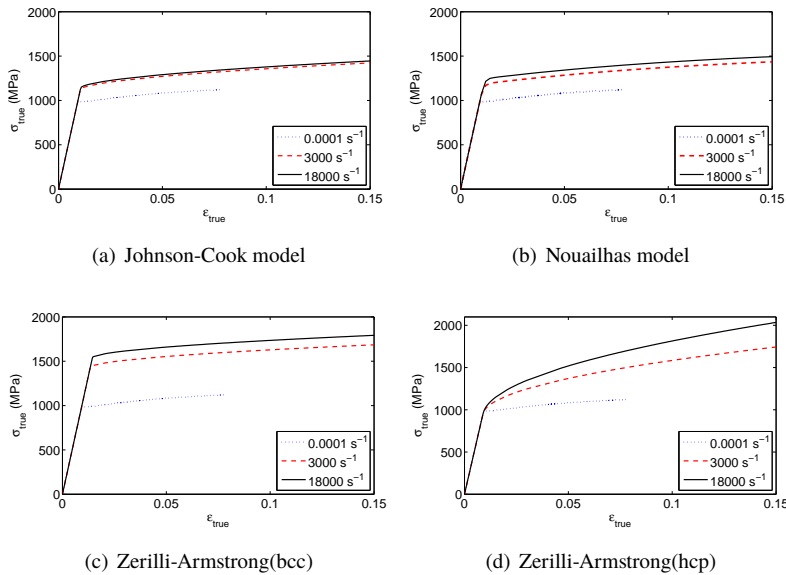


FIGURE 4: Stress-strain curves plotted within the range of  $10^{-4}$  to  $18000s^{-1}$

## 4 Conclusion

In this work, the Ti-6Al-4V has been tested on a wide range of strain rate ranging from 3000 to 25000s<sup>-1</sup> using the direct-impact Hopkinson device. An inverse analysis is carried out to identify three elastic-viscoplastic constitutive models on the dynamic experimental data. All three identified constitutive models fit well the experimental data at the strain rate ranging from 3000 up to 18000s<sup>-1</sup>. However more experimental and numerical research at higher strain rate is required to refine these results.

## Références

- [1] C. Yu, H. Gao, H. Yu, H. Jiang, and G. J. Cheng. Laser dynamic forming of functional materials laminated composites on patterned three-dimensional surfaces with applications on flexible microelectromechanical systems. *Applied Physics Letters*, 95(9) :091108, 2009.
- [2] R. M. Davies. A critical study of the Hopkinson Pressure Bar. *Philosophical Transactions of the Royal Society of London. Series A. Mathematical and Physical Sciences*, 240(821) :375–457, 1948.
- [3] H. Kolsky. An investigation of the mechanical properties of materials at very high rates of loading. *Proceedings of the Physical Society. Section B*, 62, 1949.
- [4] D. A. Gorham, P. H. Pope, and J. E. Field. An improved method for compressive stress-strain measurements at very high strain rates. *Philosophical Transactions of the Royal Society of London. Series A. Mathematical and Physical Sciences*, 438(A) :153–170, 1992.
- [5] K. T. Ramesh. Part D : Chapter 33. High strain rate and impact experiments. In *Springer handbook of experimental solid mechanics*, pp. 1–31. Springer, 2008.
- [6] C. K. H. Dharan and F. E. Hauser. Determination of stress-Strain characteristics at very high strain rates. *Experimental Mechanics*, 10(9) :370–376, 1970.
- [7] F. Kamler, P. Niessen, and R. J. Pick. Measurement of the behaviour of high-purity copper at very high rates of strain. *Canadian Journal of Physics*, 73(5–6) :295–303, 1995.
- [8] X. Guo, T. Heuzé, R. Othman, and G. Racineux. Inverse identification at very high strain rate of the Johnson–Cook constitutive model on the Ti-6Al-4V alloy with a specially designed direct-impact Kolsky bar device. *Strain*, 50(6) :527–538, 2014.
- [9] L. Wang. *Foundations of stress waves*. Elsevier BV, 2007.
- [10] X. Guo. On the direct impact Hopkinson system for dynamic tests at very high strain rates. PhD thesis, Ecole centrale de Nantes, 2015.
- [11] G. R. Johnson and W. H. Cook. A constitutive model and data for metals subjected to large strains, high strain rates and high temperatures. *Proceedings of the 7th International Symposium on Ballistics*, 21 :541–547, 1983.
- [12] Frank J. Zerilli and Ronald W. Armstrong. Constitutive relations for titanium and ti-6al-4v. In *Proceedings of the conference of the American Physical Society topical group on shock compression of condensed matter*, 370 : 315–318. AIP Publishing, 1996.
- [13] A. Andriamizeza. Rapport de stage de Master : Identification de modèles de comportement à haute vitesse de déformation sur des essais de Kolsky à impact direct. Technical report, Ecole centrale de Nantes, 2014.
- [14] D. Nouailhas. Unified modelling of cyclic viscoplasticity : application to austenitic stainless steels. *International Journal of Plasticity*, 5(5) :501–520, 1989.
- [15] R. Créac’hacdec, J. Y. Cognard, and Th. Heuzé. On modelling the non-linear behaviour of thin adhesive films in bonded assemblies with interface elements. *Journal of Adhesion Science and Technology*, 22(13) :1541–1563, 2008.
- [16] J. Lemaitre and J. L. Chaboche. *Mechanics of Solid Materials*. Cambridge University Press, 1994.